Pressure sensor based on bipolar discharge corona configuration

Article *in* Sensors and Actuators A Physical · January 2016

Impact Factor: 1.9 · DOI: 10.1016/j.sna.2015.11.024

4 authors:

Van Thanh Dau
Sumitomo Chemical
63 PUBLICATIONS **272** CITATIONS
SEE PROFILE

Bui Thanh Tung
Vietnam National University, Hanoi
54 PUBLICATIONS **153** CITATIONS
SEE PROFILE

Thien X Dinh
Ritsumeikan University
59 PUBLICATIONS **151** CITATIONS
SEE PROFILE

Tibor Terebessy
16 PUBLICATIONS **75** CITATIONS
SEE PROFILE

Sensors and Actuators A 237 (2016) 81–90

Contents lists available at ScienceDirect

Sensors and Actuators A: Physical

journal homepage: www.elsevier.com/locate/sna

Pressure sensor based on bipolar discharge corona configuration

Van Thanh Dau[a,*], Tung Thanh Bui[b], Thien Xuan Dinh[c], Tibor Terebessy[d]

[a] Research Group (Environmental Health), Sumitomo Chemical Ltd., Hyogo 665-8555, Japan
[b] Nanoelectronics Research Institute, National Institute of Advanced Industrial Science and Technology, Tsukuba 305-8568, Japan
[c] Graduate School of Science and Engineering, Ritsumeikan University, Shiga 525-8577, Japan
[d] Atrium Innovation Ltd., Lupton Road, OX10 9BT, Wallingford, United Kingdom

ARTICLE INFO

Article history:
Received 10 September 2015
Received in revised form 28 October 2015
Accepted 22 November 2015
Available online 2 December 2015

Keywords:
Bipolar corona discharge
Absolute pressure sensing
Parallel pin electrode

ABSTRACT

We present a pressure sensing unit based on a unique corona discharge setup using symmetrical electrode arrangement with simultaneous positive and negative corona generation. The device generates stable corona discharge and enables reliable air pressure measurement in the range of 80–105 kPa, tested with five prototypes. The current–voltage characteristics of bipolar discharge system is analyzed in general form and three governing parameters, namely electrode geometry, electrode distance and discharge current, are studied in relation with absolute pressure. The sensors are driven with constant discharge current as low as 1 μA. The measured sensitivity is in good agreement with theoretical prediction and the sensor stability has been confirmed with 20-h continuous test without sensitivity deterioration. The sensitivity does not depend on the tested temperature range and its variation between devices is small, approximately ±3.0%. The advantage of the proposed system compared with similar corona-based constructions is its stable operation at low current with low power consumption and minimum electrode deterioration, which provides a cost effective and reliable solution.

1. Introduction

Air pressure monitoring has widespread applications in various fields and there is a large selection of devices available based on the needs of the targeted application. Pressure sensors have been extensively applied in the automobile and aerospace industries, environmental monitoring systems, process controls, biomedical fields, and so on [1–3]. The micro-electromechanical systems (MEMS) technologies have greatly benefited from the success of the integrated circuits industry, borrowing materials, processes, and toolsets, then have been applied for sensor manufacturing, specifically pressure sensors [4]. In typical MEMS pressure sensors, the pressure is measured by piezoelectric thin films or the form of capacitance structures [5]. Commercially available micromachined pressure sensors are by a vast majority based on the piezoresistive effect, where a mechanical deformation causes a change in the electrical resistance of the sensing element which can be translated into a pressure signal. However, temperature dependence of the piezoresistive coefficient, limited pressure range and scalability have ruled out these sensors in many cases [6]. The response, sensitivity and stability are dependent on the fabrication process, which is known to be a costly investment. Moreover for absolute pressure sensing, these sensors measure the pressure relative to a high vacuum reference sealed behind its sensing diaphragm. Therefore, complex vacuum seal and packaging are compulsory [7].

Amongst the various pressure sensing principles, detecting pressure based on microdischarge properties presents a promising sensing method. Compared with other types of sensors, they offer sensitive air pressure measurement over a wider range of pressures, and the device can recover from extreme pressure shocks without permanent damage.

Devices utilizing microdischarges are particularly attractive for pressure sensing as they typically only require two electrodes for microdischarge creation. This allows them to be small, simple to fabricate, and therefore inexpensive. Up to date, micro corona discharge devices have been investigated and applied for various applications such as air flow control application [8–10], cooling applications [11–13], propulsion technology [8,14–16], micro-pump design [17,18], gas spectrometry [19,20], precipitation filtering [21–23], ozone generation [24,25], or electronic device [26–30].

The current–voltage relation of corona discharge was noticed to be altered with surrounding pressure. As pressure varies, the mean free path of ionized gas molecules changes and consequently, the discharge and current distributions vary. Utilizing these phenomena, several pressure sensing devices have been developed. Point-to-plane electrode configuration corona discharge based

* Corresponding author.
E-mail addresses: dauthanhvan@gmail.com (V.T. Dau), tung.bui@aist.go.jp (T.T. Bui), thien@cfd.ritsumei.ac.jp (T.X. Dinh), tibor.terebessy@clearviewtraffic.com (T. Terebessy).

http://dx.doi.org/10.1016/j.sna.2015.11.024
0924-4247/

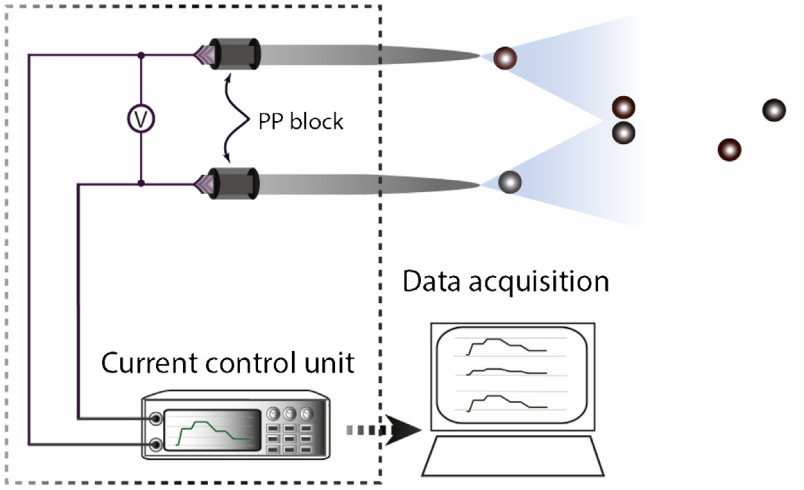

Fig. 1. Experimental setup with bipolar discharge configuration.

pressure sensing had been proposed by Chua and Son [31] for absolute pressure from 101.3 to 173.7 kPa. Béquin et al. [27] developed a corona discharge microphone, which converts acoustic pressure wave into electric signal based on the change of discharge current. In the same principle Wright [32] introduced a multi-plasma system including pressure sensor, gas purifier and chemical detector.

In this paper we present a novel and cost-effective pressure sensor, based on a unique bipolar corona system where the pressure is monitored by measuring the change in the spatial current distribution. The simultaneous production of both polarity corona discharges guarantees discharge stability in wide operational conditions. This ensures reliable operation at very low current levels (less than 1 μA), which minimizes the effect of electrode corrosion. The current–voltage relation of discharge system is first characterized by measurement and this is followed by analytical calculation of the effect of pressure on discharge properties. The pressure sensor is validated under various environmental conditions.

2. Design consideration

2.1. Current–voltage of corona discharge process

Corona discharge is typically generated at the electrode with much higher curvature, while the other electrode serves as a reference electrode. Many authors reported the characteristics of various electrode arrangements, typically they are point-to-plane [33–37], point-to-grid [38–41], point-to-ring [39,42–44], wire-to-plate [45–47], the modifications are wire-to-incline wing [13,48,49], parallel plates [50], wire-to-rod [51], rod-to-plate [52], point-to-parallel plate [53], wire-to-cylinder [54], or sphere-to-sphere [52], wire-to-wire [55], point-to-wire [40], or point-to-cylinder [56].

In these configurations, the voltage and current characteristic described in general by the empirical Townsend relationship is usually written in the form of $I/V \propto V$. This relation has originally been found in coaxial cylindrical geometry and later proven to hold for most of the configurations, point-to-plane [33,57], point-to-grid [41], point-to-ring [42].

$$I = A \times V(V - V_0) \tag{1}$$

where I is discharge current, V is applied voltage, V_0 is inception voltage for corona and A is a constant depending on electrode geometry and ion mobility μ.

Another relation, $\sqrt{I} \propto V$, which appears much less frequent in literature is assessed in the work of positive corona for point to plane with electrode distance 50 mm by Kip [58] and by Ferreira et al. [34] for negative corona with electrode distance less than 15 mm.

$$I = B \times (V - V_0)^2 \tag{2-1}$$

These results are also analyzed by Henson [33] in his work with helium vapor and by Sigmond [59] with spherically symmetric unipolar corona, where it was pointed out that Townsend low current approximation deviates from the measurement and from the more exact formula nearly from the corona onset.

Thus, in order to design a the system at low current, the current–voltage relation should be rewritten in general form $I^{1/n} \propto V$,

$$I = C\mu_0(V - V_0)^n \tag{2-2}$$

where exponent n and C depends on electrode geometry, material and electrode configurations. $\mu_0 = 2 \times 10^{-4} m^2 V^{-1} s^{-1}$ is the ion mobility in air at standard condition.

To investigate the effect of pressure, the system is assumed to be adiabatic. Under this condition, the inception voltage and ion mobility are expressed as $V_{P0} = V_0\left(P/P_0\right)^{\alpha_\vartheta}$ and $\mu_{p0} = \mu_0\left(P/P_0\right)^{\alpha_\mu}$, where $\alpha_\mu = -1/\gamma$ and $\alpha_\vartheta = 1/2\gamma$, V_0 is inception voltage evaluated at pressure $P_0 = 1.013 \times 10^5$ Pa, $\gamma \sim 1.4$ is the specific heat ratio of standard air [27].

The relation between current–voltage curve with absolute air pressure is given by.

$$I = C\mu_0\left(\frac{P}{P_0}\right)^{\alpha_\mu}\left[V - V_0\left(\frac{P}{P_0}\right)^{\alpha_\vartheta}\right]^n \tag{3-1}$$

Rearranging Eq. (3-1) with respect to V, we have

$$V = I^{\frac{1}{n}} \times (C\mu_0)^{-1/n}\left(\frac{P}{P_0}\right)^{-\alpha_\mu/n} + V_0\left(\frac{P}{P_0}\right)^{\alpha_\vartheta} \tag{3-2}$$

Accordingly, the partial relation of discharge current-pressure and voltage-pressure are

$$\frac{dI}{dP} = C\mu_0\left(\frac{1}{P_0}\right)^{\alpha_\mu}\left\{\alpha_\mu P^{\alpha_\mu - 1} \times \left[V - V_0\left(\frac{P}{P_0}\right)^{\alpha_\vartheta}\right]^n - (P)^{\alpha_\mu} \times n\left[V - V_0\left(\frac{P}{P_0}\right)^{\alpha_\vartheta}\right]^{n-1}\alpha_\vartheta V_0\left(\frac{1}{P_0}\right)^{\alpha_\vartheta} P^{\alpha_\vartheta - 1}\right\} \tag{4-1}$$

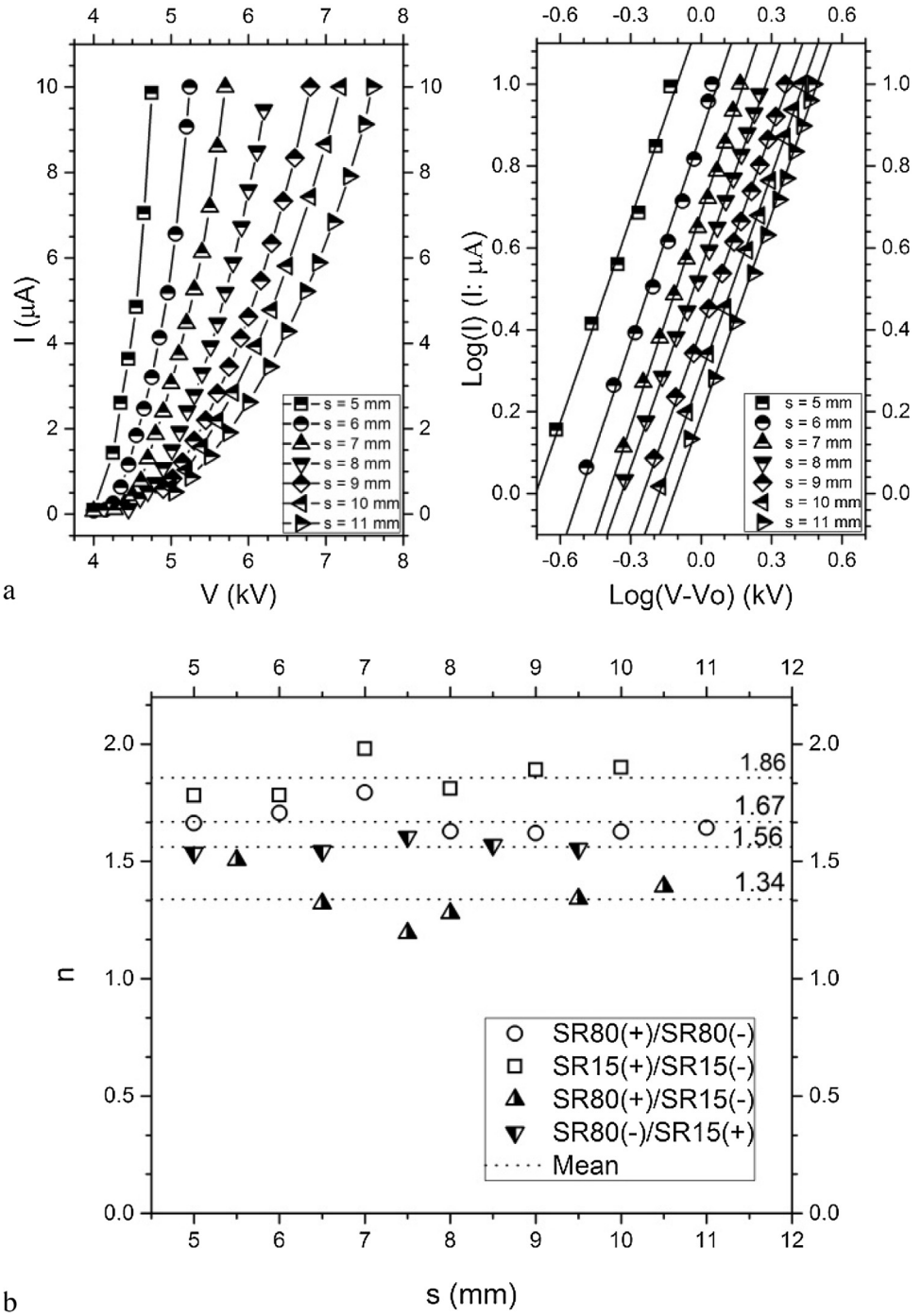

Fig. 2. (a) Measured I–V characteristic of SR80(+)/SR80(−) with varying electrode distance (left). The data is plotted in logarithmic scale with linear least square fitting lines (right). (b) Exponent *n* of configurations with SR80(+)/SR80(−); SR15(+)/SR15(−); R80(+)/SR15(−) and SR80(−)/SR15(+) shown with varying electrode distance.

$$\frac{dV}{dP} = \left[I^{1/n} (C\mu_0)^{-1/n} P_0^{\alpha_\mu/n} \right] (-\alpha_\mu/n) \times P^{\frac{-\alpha_\mu}{n}-1} + \left(\alpha_\vartheta V_0 P_0^{-\alpha_\vartheta} \right) \times P^{\alpha_\vartheta - 1} \quad (4\text{-}2)$$

Eqs. (4-1) and (4-2) represent the system measurement setup where the driving circuits are either with constant voltage or with constant current, respectively. In general, for applications using corona discharge the deterioration of electrode is always an issue affecting the device stability. An efficient method is to control and limit the discharge current, which can dramatically increase with electron avalanche under environmental influences. In our experimental setup we limited the current to values as low as several μAs. In addition, Eq. (4-1) above shows that with each value of constant voltage, the current would have complicated relation with pressure, which may result in difficulties when calibrating the device precisely.

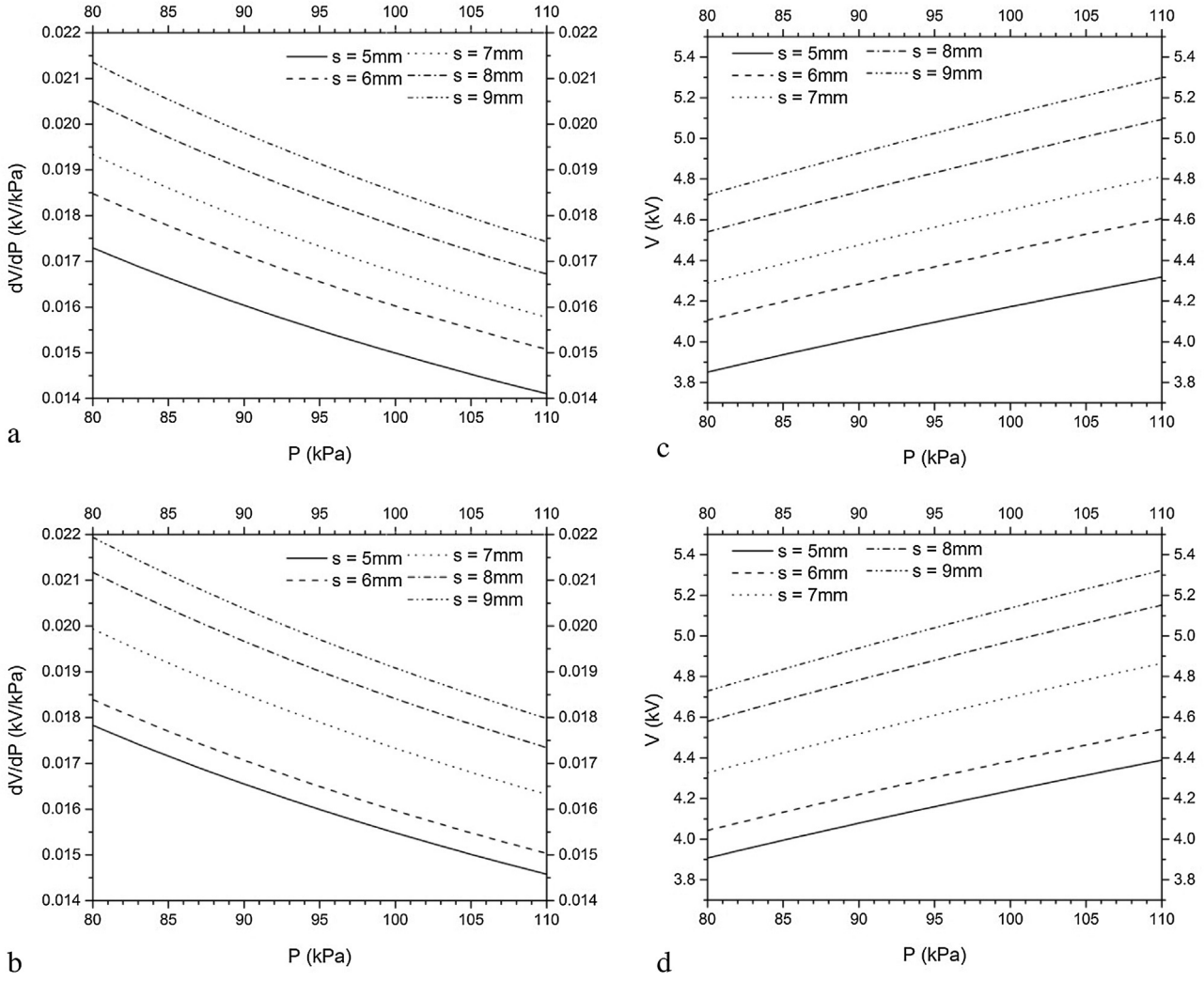

Fig. 3. (a) Relation of dV/dP versus P for configuration SR80(+)/SR80(−). (b) Relation of dV/dP versus P for configuration SR80(−)/SR15(+). (c) Relation of voltage and pressure for configuration SR80(+)/SR80(−). (d) Relation of voltage and pressure for configuration SR80(−)/SR15(+).

Therefore, at low current stage it is preferable to consider the relation between voltage and pressure while keeping the current constant. Eq. (4-2) is accordingly expressed as

$$\frac{dV}{dP} = AI^{\frac{1}{n}} \times P^{\frac{1}{n\gamma}-1} + B \times P^{\frac{1}{2\gamma}-1} \quad (5)$$

where $A = 1/n\gamma(C\mu_0)^{-1/n}P_0^{-1/n\gamma}$ and $B = 1/2\gamma V_0 P_0^{-1/2\gamma}$ are constants with fixed geometry of system.

Eq. (5) is used to describe the pressure sensor, with n ranges from 1.5 to 2 [60], which predicts that the sensitivity of voltage to pressure will reduce with increasing pressure. It also indicates that the increase of current would make the dependency of voltage on pressure more sensitive. On one hand it is a viable method to improve the sensitivity of the sensor, on the other hand high current would also increase the power consumption and accelerate the contamination of the electrode, which so far remains an unsolved challenge. While low current can give some advantages, it is unstable and has poor repeatability in common corona discharge configuration. Besides the nature of corona [61], this is also because the current appears in the system only when the discharge particles reach and are consumed at the reference electrode, otherwise the space charge at the interelectrode space quickly forms a reversed electric field and ultimately stops the corona process. This problem is successfully overcome in our configuration using bipolar corona discharge.

2.1. Design consideration of pressure sensor based on bipolar discharge system

As discussed above, the exponent n varies between positive and negative discharge, and also with the configuration of the experiment. In this part, we utilize the current–voltage characteristic of a bipolar discharge system [62], which is flexible and also stable at low current.

A viable way to build a bipolar discharge system is by simultaneously discharging from both electrodes, with opposite polarity and placed in parallel. The electrodes are connected to a single isolated power source. In this configuration, both electrodes serve as emitters and also represent the reference electrode defining the electric field, which helps the corona discharge creation simultaneously at both electrodes. Because of high recombination rate of ions [63], the oppositely charged ions originating from these electrodes neutralize each other at the interspace, thus the device is ultimately neutralized.

The experimental setup is schematically shown in Fig. 1. The symmetrical configuration is installed using two stainless steel SUS304 pins, each 8 mm long and 0.4 mm in diameter, and placed

in parallel with each other. The distance between the pins is adjustable with resolution of 0.1 mm using three axis movable stages (OptoSigma Ltd.). A high voltage generator (Kyoshin Denki Ltd.) capable of generating 10 kV direct current is used to connect to the pins. The discharge current is recorded at the negative electrode by a precision measuring circuit, which is integrated in the high voltage generator. The power unit is isolated and powered by a battery to ensure that the current measured at the negative polarity representing the creation of negative charge, is the mirror image of the current at the positive polarity for the positive charge. The system is calibrated with high voltage generator and high voltage meter (Japan Finechem Ltd.). Isolation between electrodes and stages is guaranteed by two polypropylene (PP) blocks with leak current less than 10 nA measured between the pin contact points. Because of this isolation, the current at both electrodes is equal based on Kirchhoff's current law.

Two kinds of pin tip with spherical radius (SR) approximately 80 μm and 15 μm are used. The inherent combinations are SR80(+)/SR80(−), SR15(+)/SR15(−), SR15(+)/SR80(−) and SR15(−)/SR80(+), where the signs (+) and (−) indicate voltage polarity.

Fig. 2a shows the I–V characteristics of bipolar discharge system for SR80(+)/SR80(−) configuration, the current is measured as low as 100 nA. To explore the exponent n between current and the voltage relation $I \propto (V - V_0)^n$, the measured result is examined in logarithmic scale with the least square fit (Fig. 2a, right)

$$\log(I) = n \times \log(V - V_0) + C\mu_{i0} \quad (6)$$

The exponent n is extracted from gradients in Fig. 2a (right). Similarly, the process is repeated for other combinations SR15(+)/SR15(−); SR80(+)/SR15(−) and SR80(−)/SR15(+).

Fig. 2b plots the relation between n and electrode distance. From these results, it is noticed that the exponent n depends on the pin geometry, but it is almost independent with electrode distance in the experimental range. Moreover, the configuration with two identical electrodes seems to have higher n than the asymmetric one. Clearly, when the curvature of one electrode becomes much less significant compared with the other, the bipolar electrode collapses to unipolar system whose n is approximately 1.5–1.6 depending on its charge polarity [60].

Fig. 2b gives a selection of n for pressure sensor, a sharp electrode will have lower corona onset so the device can work at lower voltage and smaller power consumption. However, it is easily defected with small distortion or contaminant, which will have considerable size with its extremely sharp tips. In reality it is also not preferable to maintain such extreme curvature for manufacturing constraints.

While the exponent n does not depend on the electrode distance, the other two parameters in Eq. (5), C and V_0, have relation with electrode distance. For each selected pin configuration, $C\mu_{i0}$ is obtained by fitting Eq. (6) with its corresponding data similar with those in Fig. 2a. With n determined from electrode geometry, $C\mu_{i0}$ and V_0 extracted from experimental data corresponding to each electrode distance, Eq. (5) is calculated. For all configurations, the discharge current is selected to be 1 μA. Fig. 3a and b expresses the relation of dV/dP versus P in configuration SR80(+)/SR80(−), $n = 1.67$, and SR80(−)/SR15(+), $n = 1.56$, respectively. Accordingly, the dependence of voltage to pressure in Eq. (3-2) is plotted in Fig. 3c and d, the theoretical sensitivity for SR80(+)/SR80(−) is from 0.015 kV/kPa to 0.018 kV/kPa with electrode distances $s = 5$ mm to $s = 9$ mm, respectively.

On one hand it is desired to keep the electrode separation to minimum, which again ensures low current operation at low voltage levels and thus minimal discharge power. In addition the generator circuit can be simplified with lower voltage levels and the risk of electrode corrosion and damage with extreme pressures is significantly reduced. On the other hand the current rises rapidly with a small voltage change above the threshold, which makes it challenging to determine the slope and thus $C\mu_{i0}$ value accurately. The precision can be improved with larger electrode separation, where the current change is more moderate with voltage variation. Based on the experimental observations and measured values, the symmetrical configuration with SR = 80 μm pin tips and electrode spacing $s = 7$ mm has been selected for further measurements presented below.

3. Pressure measurement

3.1. Experiment setup

A prototype of pressure sensor has been produced using transparent polypropylene with a mechanical precision of 20 μm, as shown in Fig. 4a. Pins are inserted into a ring-shape holder and the conventional sockets, $\varphi = 0.4$ mm, are embedded into bottom base in the bottom of the device body to serve as the placement for the pin and for reading out signal. At the tip of pin, the sensor is covered by semi-cylinder for protection. All parts are designed for press-fit structures to ensure the tolerance of mechanical assembly. A small amount of conformal coating is applied at the pin holder to ensure electric isolation. To confirm the repeatability of measurement, a total of 5 prototypes were made with same configuration and process.

For the electronics part, from the I–V characteristics presented above it is clear that although the current rise is quick once the onset voltage is reached, it is nevertheless finite and the magnitude of the voltage can be evaluated for each corresponding current value with satisfactory precision. As mentioned above, in order to reduce the effect of pin degradation over time, it is desired to limit the current to very low levels. However for practical applications, it is challenging to measure the current (e.g., by using A/D conversion) when the current is limited. A viable solution in this situation is to fix the current to a constant value (e.g., by using a comparator with input current typically much smaller than required for A/D conversion) and instead measure the voltage required for maintaining this current. Fig. 4a shows the schematics of such approach. For our experimental setup the input current to the comparator is less than 1 nA for the entire temperature range, which represents less than 1% error for current measurement. Fig. 4b shows pictures of fabricated (i) and working prototype (ii) where the bipolar corona discharge is observable at both pin electrodes. The corona glow at different discharge current is also illustrated (iii).

The device with its driving circuit is placed in pressure control chamber (MZH-05S-L, Espec Ltd.). The data is streamed to the internal memory of an onboard data acquisition at sampling rate of 1 Hz, which is then averaged for every 20 min and stored until the end of experiment.

3.2. Results and discussion

Devices are discharged with 1 μA constant current. The pressure in the test chamber varies from 80 kPa to 105 kPa with step of 5 kPa, at each step the condition is maintained for 100 min. Fig. 5a presents the data for different air pressures at standard room condition 25 °C and with absolute humidity 12.7 g/m^3. The total accumulative time for experiment is 600 min. For each individual device, the response of voltage to pressure is rather consistent and stable although small drift was noticed.

For the same measurement condition, the variance of absolute output voltage between prototypes is ±3.5% and is considered as the tolerance of device itself. The transient averaged output for each device plotted in Fig. 5b shows that the sensitivity dV/dP is

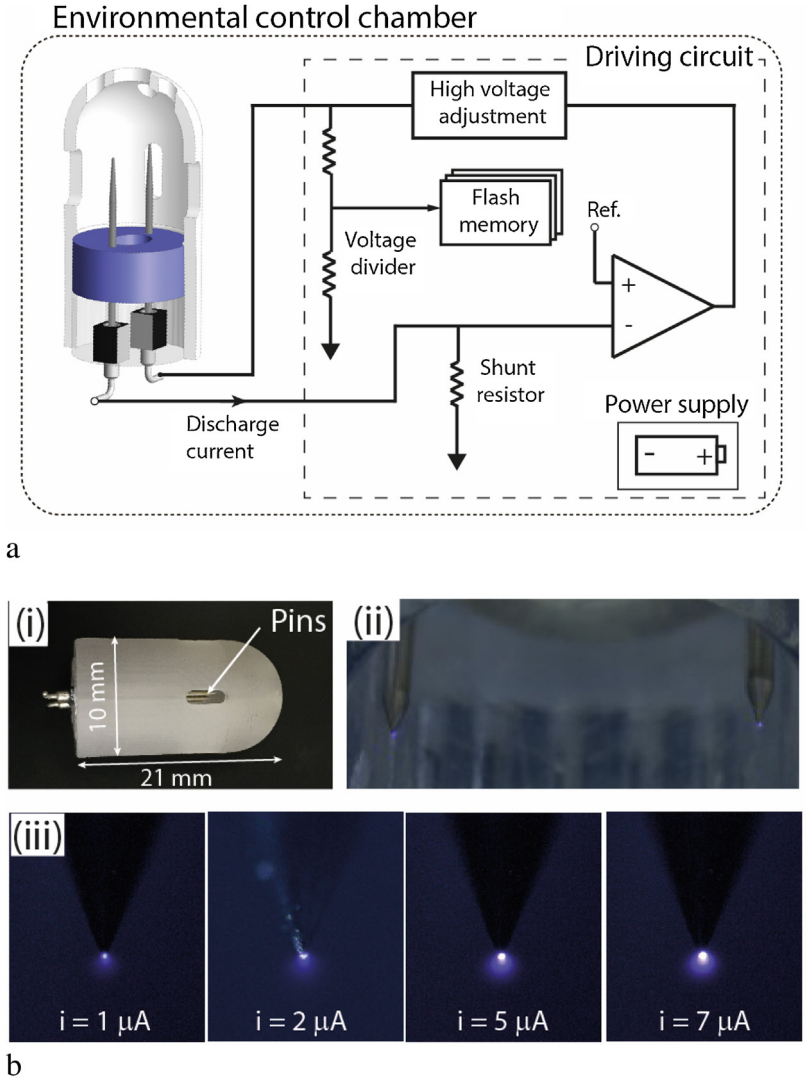

Fig. 4. (a) Schematic view of pressure sensor and its driving circuit. (b) Fabricated prototype (i) with plastic cover, a bipolar discharge during operation (ii) and corona glows at different discharge currents (iii).

0.016 kV/kPa, and is in good agreement with the theoretical prediction. In addition, the variance of sensitivity of each device is small, around ±3.0% of the average sensitivity.

The probable cause of variation between prototypes, especially the absolute value of voltage is mainly from the geometry tolerance. The electrode distance has absolute tolerance of 7.0 ± 0.15 mm, limited by our current assembly process and the tip of pin electrodes is 15–25 μm, selected from commercially claimed tolerance of 30 ± 15 μm. The initial difference between devices is considered as offset values and can be compensated with initial calibration.

It is noted that the sensitivity can be tuned by adjusting the discharge current, as predicted in Eq. (3-2), an increase in current would increase a portion of $\propto I^{1/n}$ in the sensitivity of the sensor.

For practical use, performance of sensors is also evaluated at different temperature conditions. Fig. 6a and b present data where the pressure measurement is repeated and temperature is consequently set as 15 °C and 35 °C respectively. Likewise, data is recorded at each condition for 100 min. The devices seem to be more stable at low temperature 15 °C but in general the stability of devices shows almost no change throughout the total accumulated test time of around 20 h. In addition, the sensitivity is independent with temperature. Fig. 6c plots the average output of sensor against pressure, dV/dP = 0.017 kV/kPa and 0.018 kV/kPa at 15 °C and 35 °C, respectively. These values have slight deflections with measured data at 25 °C but they are almost within the tolerance of prototypes.

Indeed, the effect of temperature to corona discharge has been widely reported [64]. The dependency of ion mobility on the temperature and pressure can be evaluated from Mason–Schamp equation describing the ion mobility as a function of temperature T and number density of drift gas N, which can be expressed using the state equation $N = P/kT$, where k is Boltzmann constant [65]. From this we can derive the relation for mobility as $\mu \propto T/P$. This relation is reflected in our device performance, which is shown in Fig. 6d. At lower temperature where the ion mobility decreases, a higher voltage is needed to maintain constant discharge current, thus the relationships V–P are linearly shifted upwards. It can be noted that as the sensitivity versus pressure does not depend on the temperature, these shifts can be compensated by integrating a conventional temperature sensor with very low cost impact.

It is also worth to mention that the inception voltage varies with measuring condition. The inception voltage in general defined by Paschen's curve depends on the product of pressure and electrode distance [66]. Too high pressure may extinguish corona while too low pressure may cause direct streamer or even spark. In our configuration the existence of proper discharge current is ensured as long as the circuit is capable of generating the required high volt-

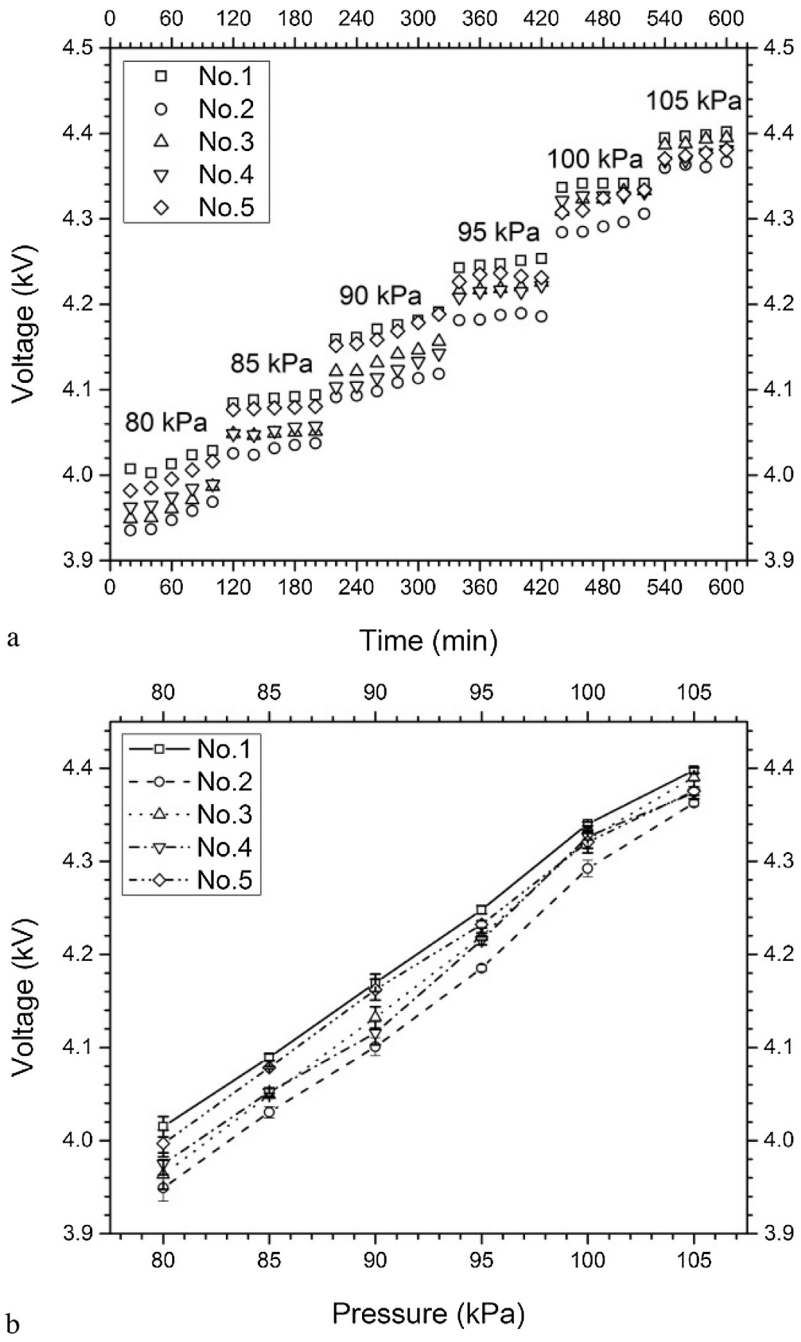

Fig. 5. (a) Relative output voltage of five devices at different pressures. The total measurement time is 10 h. (b) Transient averaged sensitivity of devices, error bar is standard deviation.

age. On the other hand, a system with fixed voltage may need to adjust voltage according to pressure range.

The power for corona discharge itself is small, around 5 mW and the power consumption of the system is less than 15 mW. Response time of the corona discharge itself to pressure change is supposed to be fast, for example around 4 kHz in the work of Béquin et al. [27], however we were not able to confirm this in our work because of the limitation from the pressure controlled chamber. In reality, delay from read-out circuit would also reduce the frequency bandwidth to several hundred hertz. If the ambient temperature cannot be pre-set and needs to be compensated for, the attached temperature sensor will also limit the time response of the device.

The total dimension of device is 21 mm × 10 mm (length × diameter). While the diameter is needed to cover a 7 mm electrode distance, there is no actual restriction to its minimum length because the length of electrode is not a governing parameter. The electrode distance is selected partly from the relative size of electrode body, which is currently 0.54 mm in diameter from its commercial availability. In reality, we believe the total size can be scaled down significantly by using smaller electrodes or by utilizing micro fabrication process.

Finally, the corona discharge depends on the gas compositions and the flow velocity, thus a recalibration is accordingly required. In addition, a suitable housing to prevent flow from directly moving across sensor probe is needed.

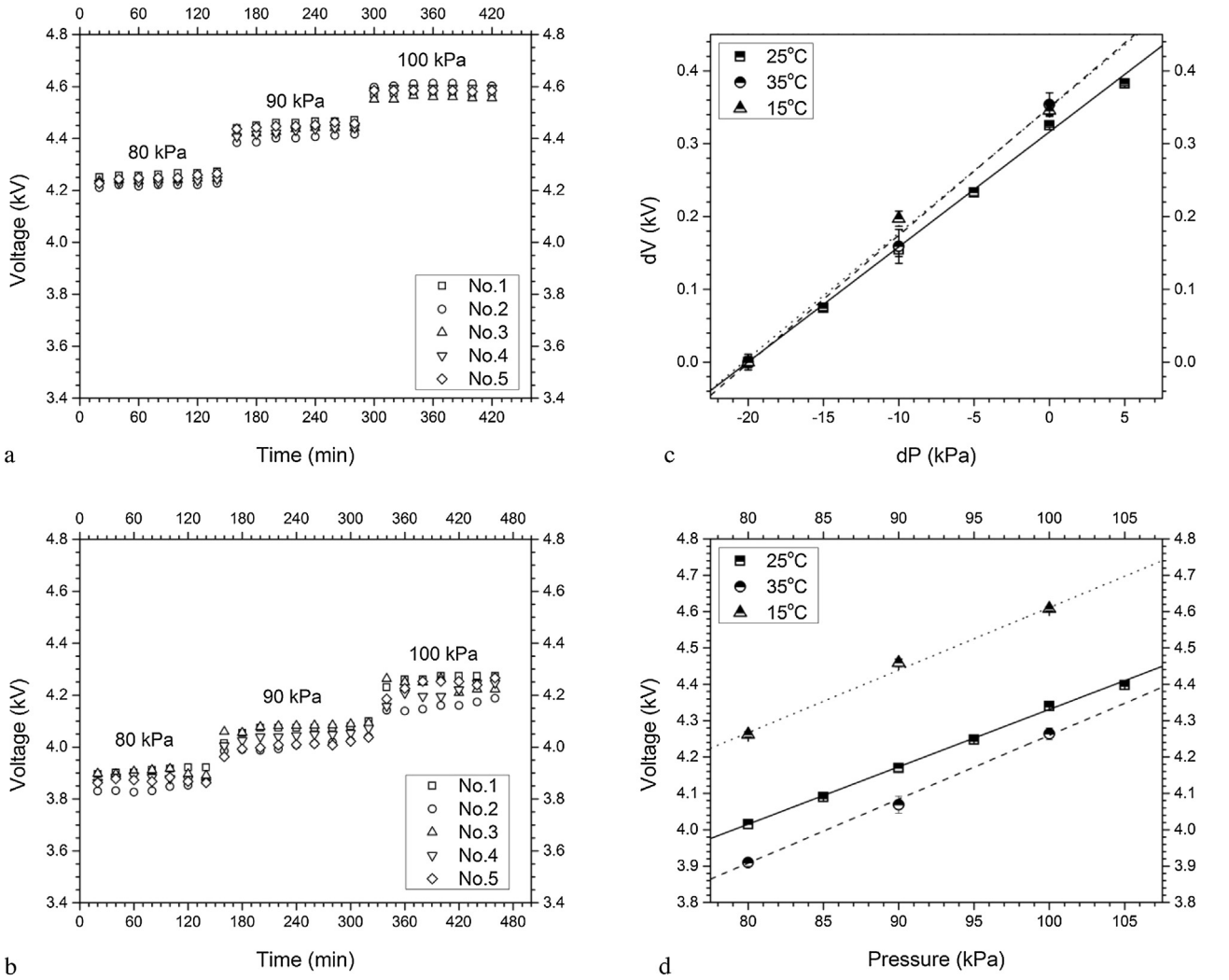

Fig. 6. (a) Output voltage versus pressure at 15 °C. (b) Output voltage versus pressure at 35 °C. (c) Relative output of sensors at different temperatures, error bar is standard deviation and lines are linear fitting. (d) Output voltage versus pressure at different temperatures. Error bar is standard deviation, lines are linear fitting.

4. Conclusion

We have presented an absolute pressure sensor based on unique bipolar corona discharge. The configuration is based on the simultaneous generation of both positive and negative ions using two sharp electrodes placed in parallel, thus the device is neutralized by itself and allows stable discharge operation at sub-microampere current levels. The current–voltage characteristics of bipolar discharge system has been analysed in general form. Three governing parameters; electrode geometry, electrode distance and driving current, have been studied in relation with absolute pressure.

Five prototypes have been made and tested in pressure range of 80–105 kPa. The sensors were driven with constant discharge current, which is set low but stable enough to ensure the existence of corona discharge. The measured sensitivity is in good agreement with theoretical prediction and the sensor stability has been confirmed in 20-h continuous operation without sensitivity deterioration. The sensitivity does not depend on tested temperature range and its variation between devices is small, approximately ±3.0%. The advantage of the proposed system compared with similar corona-based constructions is its stable operation at low current with low power consumption, and negligible electrode deterioration providing a cost effective and reliable solution. Because both electrodes have minimal size, this also allows the use of noble metals as electrode material to enhance the performance without significant cost increase.

References

[1] T. Someya, T. Sekitani, S. Iba, Y. Kato, H. Kawaguchi, T. Sakurai, A large-area, flexible pressure sensor matrix with organic field-effect transistors for artificial skin applications, Proc. Natl. Acad. Sci. U. S. A. 101 (2004) 9966–9970, http://dx.doi.org/10.1073/pnas.0401918101.
[2] M. Kraft, N.M. White, Mems for Automotive and Aerospace Applications, 1st ed., Elsevier, 2013, 2015.
[3] R. Bogue, MEMS sensors: past, present and future, Sen. Rev. 27 (2007) 7–13, http://dx.doi.org/10.1108/02602280710729068.
[4] S. Beeby, MEMS Mechanical Sensors, 9781580538732, 2004.
[5] W.P. Eaton, J.H. Smith, E. Ed, Micromachined pressure sensors: review and recent developments, Smart Mater. Struct. 6 (1997) 530–539, http://dx.doi.org/10.1088/0964-1726/6/5/004.
[6] W. Barlian, J.R. Mallon Jr, A.J. Rastegar, B.L. Pruitt, Review: semiconductor piezoresistance for microsystems, Proc. IEEE Inst. Electr. Electron. Eng. (2009) 513–552, http://dx.doi.org/10.1109/JPROC.2009.2013612, Review.
[7] P.K. Rathore, J. Akhtar, Fabrication of a membrane type double cavity vacuum-sealed micro sensor for absolute pressure based on front-side lateral etching technology, Sen. Rev. 31 (2011) 41–46, http://dx.doi.org/10.1108/02602281111099071.
[8] E. Moreau, Airflow control by non-thermal plasma actuators, J. Phys. D Appl. Phys. 40 (2007) 605–636, http://dx.doi.org/10.1088/0022-3727/40/3/s01.
[9] T.C. Corke, C.L. Enloe, S.P. Wilkinson, Dielectric barrier discharge plasma actuators for flow control*, Annu. Rev. Fluid Mech. 42 (2010) 505–529, http://dx.doi.org/10.1146/annurev-fluid-121108-145550.

[10] D.F. Opaits, Dielectric barrier discharge plasma actuator for flow control final report, NASA Rep. NASA/CR (2012).
[11] D.B. Go, T.S. Fisher, S.V. Garimella, Direct simulation of ionization and ion transport for planar microscale ion generation devices, J. Phys. D Appl. Phys. 42 (2009) 55203, http://dx.doi.org/10.1088/0022-3727/42/5/055203.
[12] K.G. Kibler, H.G. Carter, Electrocooling in gases, J. Appl. Phys. 45 (1974) 4436–4440, http://dx.doi.org/10.1063/1.1663069.
[13] A. Rashkovan, E. Sher, H. Kalman, Experimental optimization of an electric blower by corona wind, Appl. Therm. Eng. 22 (2002) 1587–1599, http://dx.doi.org/10.1016/s1359-4311(02) 00082-0.
[14] A.A. Martins, Modelling of an improved positive corona thruster and actuator, J. Electrostat. 71 (2013) 61–67, http://dx.doi.org/10.1016/j.elstat.2012.09.001.
[15] L. Zhao, K. Adamiak, Numerical analysis of forces in an electrostatic levitation unit, J. Electrostat. 63 (2005) 729–734, http://dx.doi.org/10.1016/j.elstat.2005.03.036.
[16] A.A. Martins, M.J. Pinheiro, On the influence that the ground electrode diameter has in the propulsion efficiency of an asymmetric capacitor in nitrogen gas, Phys. Plasmas 18 (2011) 33512, http://dx.doi.org/10.1063/1.3562874.
[17] O.M. Stuetzer, Ion drag pumps, J. Appl. Phys. 31 (1960) 136–146, http://dx.doi.org/10.1063/1.1735388.
[18] M. Rickard, D. Dunn-Rankin, F. Weinberg, F. Carleton, Characterization of ionic wind velocity, J. Electrostat. 63 (2005) 711–716, http://dx.doi.org/10.1016/j.elstat.2005.03.033.
[19] D.F. Colas, A. Ferret, D.Z. Pai, D.A. Lacoste, C.O. Laux, Ionic wind generation by a wire-cylinder-plate corona discharge in air at atmospheric pressure, J. Appl. Phys. 108 (2010) 0–6, http://dx.doi.org/10.1063/1.3514131.
[20] D.I. Carroll, I. Dzidic, R.N. Stillwell, K.D. Haegele, E.C. Horning, Atmospheric pressure ionization mass spectrometry. Corona discharge ion source for use in a liquid chromatograph-mass spectrometer-computer analytical system, Anal. Chem. 47 (1975) 2369–2373, http://dx.doi.org/10.1021/ac60364a031.
[21] H. Ait Said, H. Nouri, Y. Zebboudj, Effect of air flow on corona discharge in wire-to-plate electrostatic precipitator, J. Electrostat. 73 (2015) 19–25, http://dx.doi.org/10.1016/j.elstat.2014.10.004.
[22] B. Chua, A.S. Wexler, N.C. Tien, D.A. Niemeier, B.A. Holmén, Micro corona based particle steering air filter, Sens. Actuators A Phys. 196 (2013) 8–15, http://dx.doi.org/10.1016/j.sna.2013.03.029.
[23] B. Chua, A.S. Wexler, N.C. Tien, D.A. Niemeier, B.A. Holm, Collection of liquid phase particles by microfabricated electrostatic precipitator, J. Microelectromech. Syst. 22 (2013) 1010–1019.
[24] M. Meziane, O. Eichwald, J.P. Sarrette, O. Ducasse, M. Yousfi, F. Marchal, Electro-hydrodynamics and kinetic modelling of polluted air flow activated by multi-tip-to-plane corona discharge, J. Appl. Phys. 113 (2013), http://dx.doi.org/10.1063/1.4801879.
[25] B. Chua, A.S. Wexler, N.C. Tien, D.A. a, B. Niemeier, Design, fabrication, and testing of a microfabricated corona ionizer, J. Microelectromech. Syst. 17 (2008) 115–123, http://dx.doi.org/10.1109/jmems.2007.909515.
[26] B. Chua, J.J. Pak, Miniaturized corona flow sensor operating in drift mobility increment mode for low flow velocity measurement, Sens. Actuators A Phys. 224 (2015) 65–71, http://dx.doi.org/10.1016/j.sna.2015.01.022.
[27] P. Béquin, V. Joly, P. Herzog, Modeling of a corona discharge microphone, J. Phys. D Appl. Phys. 46 (2013) 175204, http://dx.doi.org/10.1088/0022-3727/46/17/175204.
[28] T.H. Kim, S.J. Kim, Development of a helium flow sensor based on dielectric barrier discharge at atmospheric pressure, Sens. Actuators A Phys. 167 (2011) 297–303, http://dx.doi.org/10.1016/j.sna.2011.02.054.
[29] B. Chua, A.S. Wexler, N.C. Tien, D.A. Niemeier, B.A. Holmen, Electrical mobility separation of airborne particles using integrated microfabricated corona ionizer and separator electrodes, J. Microelectromech. Syst. 18 (2009) 4–13, http://dx.doi.org/10.1109/JMEMS.2008.2011123.
[30] E.-H. Lee, B. Chua, A. Son, Micro corona discharge based cell lysis method suitable for inhibitor resistant bacterial sensing systems, Sens. Actuators B Chem. 216 (2015) 17–23, http://dx.doi.org/10.1016/j.snb.2015.04.030.
[31] B. Chua, A. Son, Sensing absolute air pressure using micro corona discharge, Sens. Actuators A Phys. 217 (2014) 49–55, http://dx.doi.org/10.1016/j.sna.2014.06.025.
[32] S.A. Wright, Microdischarge-Based Pressure Controlling Devices and Their Applications to Chemical Sensing in Harsh Environments, The University of Michigan, 2009.
[33] B.L. Henson, Toward a fundamental model for steady point-plane corona discharges, J. Appl. Phys. 55 (1984) 150–157, http://dx.doi.org/10.1063/1.332878.
[34] G.F.L. Ferreira, O.N. Oliveira, J.A. Giacometti, Point-to-plane corona: current-voltage characteristics for positive and negative polarity with evidence of an electronic component, J. Appl. Phys. 59 (1986) 3045–3049, http://dx.doi.org/10.1063/1.336926.
[35] D. Bessierres, J. Paillol, N. Soulem, Negative corona triggering in air, J. Appl. Phys. 95 (2004) 3943–3951, http://dx.doi.org/10.1063/1.1667599.
[36] J. Zhang, F.C. Lai, Effect of emitting electrode number on the performance of EHD gas pump in a rectangular channel, J. Electrostat. 69 (2011) 486–493, http://dx.doi.org/10.1016/j.elstat.2011.06.007.
[37] H. Kawamoto, H. Yasuda, S. Umezu, Flow distribution and pressure of air due to ionic wind in pin-to-plate corona discharge system, J. Electrostat. 64 (2006) 400–407, http://dx.doi.org/10.1016/j.elstat.2005.10.023.
[38] A. Ongkodjojo Ong, A.R. Abramson, N.C. Tien, Electrohydrodynamic microfabricated ionic wind pumps for thermal management applications, J. Heat Transfer 136 (2014) 61703, http://dx.doi.org/10.1115/1.4026807.
[39] M. Rickard, D. Dunn-Rankin, F. Weinberg, F. Carleton, Maximizing ion-driven gas flows, J. Electrostat. 64 (2006) 368–376, http://dx.doi.org/10.1016/j.elstat.2005.09.005.
[40] I.Y. Chen, M.Z. Guo, K.S. Yang, C.C. Wang, Enhanced cooling for LED lighting using ionic wind, Int. J. Heat Mass Transfer 57 (2013) 285–291, http://dx.doi.org/10.1016/j.ijheatmasstransfer.2012.10.015.
[41] K. Yamada, An empirical formula for negative corona discharge current in point-grid electrode geometry, J. Appl. Phys. 96 (2004) 2472–2475, http://dx.doi.org/10.1063/1.1775301.
[42] P. Giubbilini, The current-voltage characteristics of point-to-ring corona, J. Appl. Phys. 64 (1988) 3730–3732, http://dx.doi.org/10.1063/1.341368.
[43] H. Kawamoto, S. Umezu, Electrostatic micro-ozone fan that utilizes ionic wind induced in pin-to-plate corona discharge system, J. Electrostat. 66 (2008) 445–454, http://dx.doi.org/10.1016/j.elstat.2008.04.009.
[44] A.M. Drews, L. Cademartiri, G.M. Whitesides, K.J.M. Bishop, Electric winds driven by time oscillating corona discharges, J. Appl. Phys. 114 (2013), http://dx.doi.org/10.1063/1.4824748.
[45] D.B. Go, S.V. Garimella, T.S. Fisher, R.K. Mongia, Ionic winds for locally enhanced cooling, J. Appl. Phys. 102 (2007), http://dx.doi.org/10.1063/1.2776164.
[46] R. Tirumala, Y. Li, D.A. Pohlman, D.B. Go, Corona discharges in sub-millimeter electrode gaps, J. Electrostat. 69 (2011) 36–42, http://dx.doi.org/10.1016/j.elstat.2010.10.006.
[47] Y. Zebboudj, R. Ikene, Positive corona inception in HVDC configurations under variable air density and humidity conditions, Eur. Phys. J. Appl. Phys. 10 (2000) 211–218, http://dx.doi.org/10.1051/epjap:2000134.
[48] C. Kim, K.C. Noh, J. Hyun, S.G. Lee, J. Hwang, H. Hong, Microscopic energy conversion process in the ion drift region of electrohydrodynamic flow, Appl. Phys. Lett. 100 (2012), http://dx.doi.org/10.1063/1.4729443.
[49] H. Tsubone, G.D. Harvel, K. Urashima, J.S. Chang, H. Tsubone, G.D. Harvel, et al., Narrow-flow-channel-driven EHD gas pump for an advanced thermal management of microelectronics, IEEE Trans. Ind. Appl. 46 (2010) 1151–1158, http://dx.doi.org/10.1109/TIA.2010.2045326.
[50] P.J. McKinney, J.H. Davidson, D.M. Leone, Current distributions for barbed plate-to-plane coronas, IEEE Trans. Ind. Appl. 28 (1992) 1424–1431, http://dx.doi.org/10.1109/28.175297.
[51] B. Komeili, J.S. Chang, G.D. Harvel, C.Y. Ching, D. Brocilo, Flow characteristics of wire-rod type electrohydrodynamic gas pump under negative corona operations, J. Electrostat. 66 (2008) 342–353, http://dx.doi.org/10.1016/j.elstat.2008.02.004.
[52] H. Toyota, S. Zama, Y. Akamine, S. Matsuoka, K. Hidaka, Gaseous electrical discharge characteristics in air and nitrogen at cryogenic temperature, IEEE Trans. Dielectr. Electr. Insul. 9 (2002) 891–898, http://dx.doi.org/10.1109/tdei.2002.1115482.
[53] D.H. Shin, J.S. Yoon, H.S. Ko, Experimental optimization of ion wind generator with needle to parallel plates for cooling device, Int. J. Heat Mass Transfer 84 (2015) 35–45, http://dx.doi.org/10.1016/j.ijheatmasstransfer.2015.01.018.
[54] B. Kim, S. Lee, Y.S. Lee, K.H. Kang, Ion wind generation and the application to cooling, J. Electrostat. 70 (2012) 438–444, http://dx.doi.org/10.1016/j.elstat.2012.06.002.
[55] J. Darabi, C. Rhodes, CFD modeling of an ion-drag micropump, Sens. Actuators A Phys. 127 (2006) 94–103, http://dx.doi.org/10.1016/j.sna.2005.10.051.
[56] L. Li, S.J. Lee, W. Kim, D. Kim, An empirical model for ionic wind generation by a needle-to-cylinder dc corona discharge, J. Electrostat. 73 (2015) 125–130, http://dx.doi.org/10.1016/j.elstat.2014.11.001.
[57] M. Robinson, Movement of air in the electric wind of the corona discharge, Trans. Am. Inst. Electr. Eng. I Commun. Electron. 80 (1961) 143–150, http://dx.doi.org/10.1109/tce.1961.6373091.
[58] A.F. Kip, Onset studies of positive point-to-plane corona in air at atmospheric pressure, Phys. Rev. 55 (1939) 549–556, http://dx.doi.org/10.1103/physrev.55.549.
[59] R.S. Sigmond, Simple approximate treatment of unipolar space-charge-dominated coronas: the Warburg law and the saturation current, J. Appl. Phys. 53 (1982) 891–898, http://dx.doi.org/10.1063/1.330557.
[60] X. Meng, H. Zhang, J. (Jesse) Zhu, A general empirical formula of current?voltage characteristics for point-to-plane geometry corona discharges, J. Phys. D Appl. Phys. 41 (2008) 065209, http://dx.doi.org/10.1088/0022-3727/41/6/065209.
[61] J.S. Chang, P.A. Lawless, T. Yamamoto, Corona discharge processes, IEEE Trans. Plasma Sci. 19 (1991) 1152–1166, http://dx.doi.org/10.1109/27.125038.
[62] Z.M. Al-Hamouz, Corona power loss, electric field, and current density profiles in bundled horizontal and vertical bipolar conductors, IEEE Trans. Ind. Appl. 38 (2002) 1182–1189, http://dx.doi.org/10.1109/tia.2002.802931.
[63] B.M. Smirnov, H.S.W. Massey Sr., Negative Ions, McGraw-Hill Companies, 1982.
[64] M. Tabrizchi, F. Rouholahnejad, Comparing the effect of pressure and temperature on ion mobilities, J. Phys. D Appl. Phys. 38 (2005) 857–862, http://dx.doi.org/10.1088/0022-3727/38/6/012.
[65] E.A. Mason, Ion mobility its role in plasma chromatography 1984.
[66] Y.P. Raizer, J.E. Allen, V.I. Kisin, Gas Discharge Physics, Springer, 2011.

Biographies

Van Thanh Dau received the B.S. degree in aerospace engineering from Hochiminh City University of Technology, Vietnam, in 2002, and the M.S. and Ph.D. degrees in micromechatronics from Ritsumeikan University, Japan, in 2004 and 2007, respectively. From 2007 to 2009, he was a Postdoctoral Fellow with Japan Society for the Promotion of Science (JSPS) at Micro Nano Integrated Devices Laboratory, Ritsumeikan University. Since 2010 he has been with Research Group, Sumitomo Chemical Co. Ltd., where he works on integrated micro electrospray and atomization methods. His current research subjects are micro fluidics, electro hydrodynamics, microsensors and microactuators. He is the author and co-author of more than 70 scientific articles and 17 inventions.

Tung Thanh Bui received the B.S. degree in electrical engineering from Vietnam National University, Hanoi (VNUH) in 2004, and the M.E. and D.Eng. degrees in Science and Engineering from Ritsumeikan University, Shiga, Japan, in 2008 and 2011, respectively. Since 2011 he has been a Post-doctoral Researcher with the 3D Integration System Group, Nanoelectronics Research Institute (NeRI), National Institute of Advanced Industrial Science and Technology (AIST), Tsukuba, Japan. His current research interests are 3D system integration technology and MEMS based sensors, actuators and applications. He is the author and co-author of more than 60 scientific articles and 7 inventions.

Thien Xuan Dinh received the B.S. degree in aerospace engineering fromHochiminh City University of Technology in 2002, Vietnam and the M.Sc. and Ph.D. degrees in mechanical engineering from Ritsumeikan University in 2004 and 2007, respectively. He was recipient of Japan Government Scholarship (MEXT) for Outstanding Student to pursuits his M. Sc. and Ph. D. courses and Japan Society for the Promotion of Science postdoctoral fellowship from 2011 to 2013. His general research interest is computation of fluid flow. The large parts of his research are turbulence modeling using Large Eddy Simulation, multiphase modeling using Volume of Fluid technique, and simulation of turbulence and dispersion. Recently, he has focused on computation of fluid flow for developing microfluidic devices as microsensors, micropump, and micromixer for biochemical engineering.

Tibor Terebessy received his M.S. degree with honour in plasma physics from Comenius University, Slovakia, in 1998 and his Ph.D. degree in electronics engineering from Shizuoka University, Japan, in 2002. He was then awarded a Postdoctoral Fellowship by the Japan Society for the Promotion of Science (JSPS), continuing his research in large area microwave discharges and their industrial applications at Graduate School of Electronic Science and Technology, Shizuoka University, Japan. His main areas of research interests include atmospheric pressure discharges, microwave plasmas, nanoparticle generation and electrohydrodynamics. He is the author and co-author of more than 20 scientific articles and 17 inventions.